Microchimica Acta (2025) 192:417
https://doi.org/10.1007/s00604-025-07289-5

RESEARCH

Orthogonal CRISPR/Cas system facilitated dual-color fluorescence fiber-embedded optofluidic nano-biochip for parallel amplification-free on-site detection of bacterium and virus

Dan Song[1,2] · Wenjuan Xu[1] · Yuxin Zhuo[1] · Anna Zhu[3] · Feng Long[1]

Received: 21 March 2025 / Accepted: 28 May 2025

Abstract

Bacterial and viral co-infections significantly exacerbate morbidity and mortality. Rapid, sensitive, and parallel detection of these pathogens remains a critical challenge. Here, an orthogonal **C**RISPR/Cas system facilitated **d**ual-color fluorescence **f**iber-embedded **o**ptofluidic nano-**b**iochip (CD-FOB) was fabricated. Leveraging the time-resolved effect, the CD-FOB achieved ultrasensitive parallel detection of *Escherichia coli* O157:H7 (*E. coli* O157:H7) and SARS-CoV-2 based on a multiple signal enhancement strategy, including the collateral cleavage activity of CRISPR/Cas, evanescent wave fluorescence enhancement, DNA-mediated signal amplification, and air-displacement fluorescence enhancement. Without the need for amplification, the CD-FOB system has a detection limit of 643 CFU/mL for *E. coli* O157:H7 and 3.48 copies/μL for SARS-CoV-2 within 50 min analysis time. To enable rapid on-site detection, a lyophilized CRISPR/Cas assay was prepared using stabilized freeze-dried reagents for detecting *E. coli* O157:H7 and SARS-CoV-2 in actual samples, achieving recoveries ranging from 70.5% to 200.5%. The unique combination of technical simplicity, multiplexing capability, and operational robustness positions CD-FOB as a versatile solution for combating current and future pathogen threats.

Graphical Abstract

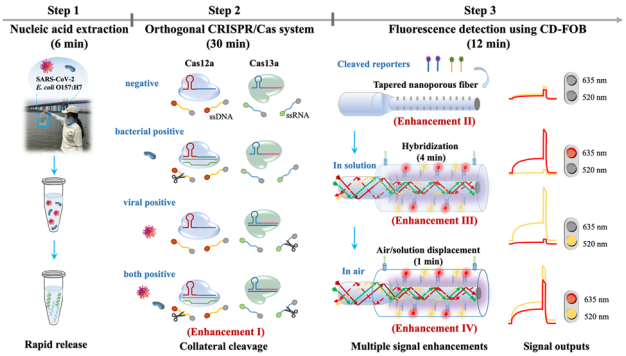

Keywords Orthogonal CRISPR/Cas system · Fiber embedded optofluidic nanochip · Dual color fluorescence system · *Escherichia coli* O157:H7 · SARS-CoV-2

✉ Feng Long
longf04@ruc.edu.cn

[1] School of Environment and Natural Resources, Renmin University of China, Beijing 100872, China

[2] School of Environment, Tsinghua University, Beijing 100084, China

[3] State Key Laboratory of NBC Protection for Civilian, Beijing 102205, China

Introduction

Bacteria and viruses, two distinct categories of microorganisms, are prevalent in nature and can cohabit various settings, including the human body, environments such as soil and water, and wastewater treatment facilities [1–4]. Significant interplay between bacterial and viral infections is

Published online: 12 June 2025

crucial for disease onset and progression [5, 6]. Bacteria promote viral infections by suppressing the host immunity [7], increasing adhesion proteins [8], and activating viral proteins [9]. Conversely, viruses facilitate bacterial co-infections by weakening immune defenses [10], damaging epithelial barriers [11], inducing receptor expression [12], and directly binding bacteria [13]. For instance, influenza A virus can bind directly to bacteria, increasing their adherence to host cells and raising mortality risk [14]. Studies suggested that the high morbidity rates during the 1918 influenza pandemic might originate from secondary bacterial pneumonia [15]. Similarly, during the COVID-19 pandemic, a parallel trend was observed that secondary bacterial infections raised mortality from 18.7% to 50% [16]. Owing to these bacterial coinfections, there has been a surge in morbidity rates and mortality rates associated with viral infections.

Rapid and precise detection of bacteria and viruses is a vital first step in preventing the spread of infectious diseases and mitigating health risks [17–19]. While culture methods remain the reference standard, their long turnaround (> 24 h), technical requirements, and proneness to false-negative results limit their utility. Immunoassays allow point-of-care detection of pathogens but suffer from inadequate sensitivity and are limited to a few common bacteria or viruses. Real-time reverse transcription-polymerase chain reaction (RT-PCR) provides the gold standard method for pathogen detection, but involves intensive sample pretreatment and contamination problems [20–22]. Multiplex qPCR technology is most commonly used technique for the simultaneous detection of multiple viruses or bacteria, which uses multiple sets of primers and probes in a single reaction to detect and differentiate among various pathogens [23, 24]. Though PCR-based amplification methods have been successfully implemented in point-of-care testing systems, multiplex detection requires more precise primer design to avoid cross-reactivity [25, 26].

The emergence of clustered regularly interspaced short palindromic repeats/CRISPR-associated protein (CRISPR/Cas) systems has revolutionized pathogen detection [27–29]. Numerous CRISPR-based biosensors (e.g., SHERLOCK, DETECTR, HOLMES) have been constructed and multiplexed CRISPR/Cas platforms aroused broad interest in addressing high throughout needs [30–33]. Orthogonal CRISPR/Cas systems utilizing distinct *trans*-cleavage activities of Cas effectors is common approach for multiplexed detection [34, 35]. However, current systems fail in achieving high sensitivity and cost-effectiveness. While conventional multiplex quantitative PCR offers high sensitivity, it requires expensive specialized equipment. Conversely, portable detection platforms often lack sufficient sensitivity and need additional nucleic acid amplification steps. This trade-off between analytical performance and practical applicability remains a critical challenge in point-of-care diagnostics. Researchers are increasingly integrating machine learning algorithms to optimize detection accuracy and improve system reliability [36]. Currently, exploring CRISPR/Cas-based detection devices without nucleic acid amplification is a continuous effort [37, 38]. Nevertheless, these methods are inadequate for high-throughput parallel on-site detection due to reliance on bulky instrumentation (e.g., plate readers or microscopes), lack of integrated sample-to-result workflows, and limited multiplexing capacity. Amplification-free detection demand exceptional sensitivity, while current platforms typically analyze targets sequentially, severely limiting their utility for rapid, high-throughput pathogen screening.

To address these concerns, an orthogonal CRISPR−Cas12a/Cas13a facilitated dual-color fluorescence fiber-embedded optofluidic bio-nano-chip (CD-FOB) was constructed for parallel amplification-free on-site detection of bacteria and viruses (Fig. 1). Unlike traditional optofluidic systems which achieve parallel analysis based on spatial separation or various labels with high cost and complexity, the CD-FOB employs a compact all-fiber optical structure that eliminates precise optical alignment requirements [39–41]. The fiber-embedded optofluidic bio-nano-chip is constructed by embedding a functionalized fiber nano-biosensor into an optofluidic chip, which acts as both a biorecognition element and an optical transmission and signal enhancement element. The CD-FOB was validated for parallel detection of *E. coli* O157:H7 and SARS-CoV-2 using the orthogonal CRISPR−Cas12a/Cas13a system. The two pathogens can be excreted through the feces of infected individuals and pose fecal–oral transmission risk in water systems [42, 43]. The CD-FOB achieved sensitive parallel quantification of *E. coli* O157:H7 and SARS-CoV-2 through multiple signal enhancements. Lyophilized reagents were prepared to realize sample-to-result analysis. This integrated platform represents a powerful tool for high-throughput, on-site parallel detection of diverse pathogens, addressing critical needs in global pathogen surveillance.

Experimental sections

Reagents and apparatus

The *rfbE* gene plasmid of *E. coli* O157:H7 was constructed by Hanbio Biotechnology Co. Ltd (Shanghai, China). FNV-SARS-CoV-2-abEN (Cat. BDAA0004) with partial ORF1a/b gene sequences, complete E gene, and complete N gene was purchased from Beijing Biodragon Immunotechnologies Co., Ltd. (Beijing, China). LbCas12a nuclease (Cat. 32,108) and LwaCas13a nuclease (Cat. 32,117) were purchased from Tolo Biotech (Shanghai, China). Oligonucleotides used in the experiment were synthesized by Sangon Biotech Co. (Shanghai, China), and the sequences are shown in Table S1.

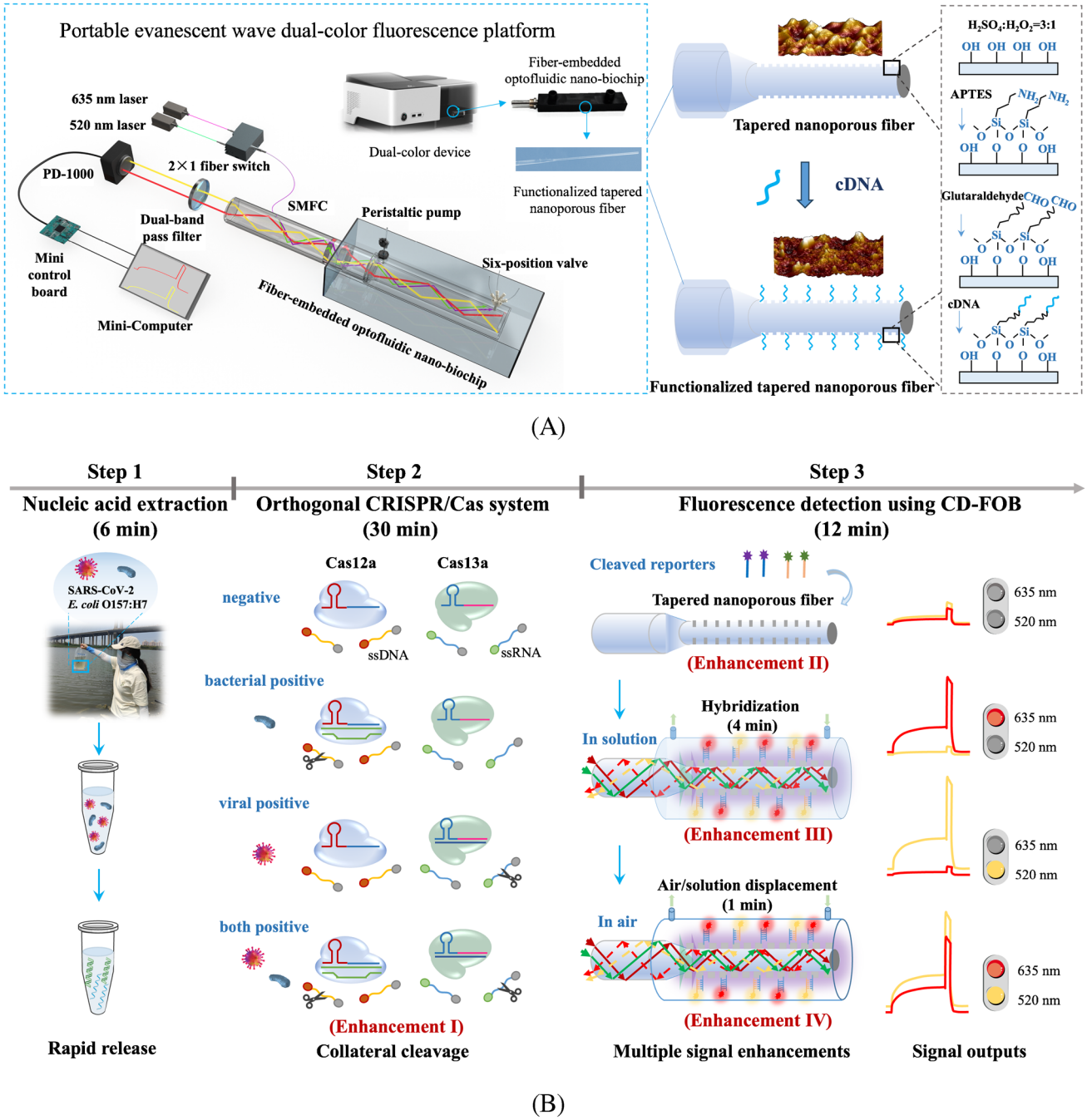

Fig. 1 Parallel detection mechanism of bacteria and viruses using CRISPR/Cas facilitated CD-FOB based on multiple signal enhancements. **A** Schematic diagram of the portable evanescent wave dual-color fluorescence detection device and the fiber-embedded optofluidic nano-biochip with the preparation process of the functionalized fiber nano-biosensor. **B** Parallel detection mechanism of *E. coli* O157:H7 and SARS-CoV-2 using orthogonal CRISPR/Cas facilitated CD-FOB with multiple signal enhancements

The RNase inhibitor (Cat. R8061) was obtained from Beijing Solarbio Science & Technology Co. Ltd (Beijing, China). *S. aureus* strain ATCC25923, *L. monocytogenes* ATCC19115, and *E. coli* O157:H7 were purchased from the Bena Culture Collection (BNCC, China). A universal nucleic acid (DNA/RNA) rapid release reagent (Cat. WLDR8202) was obtained from Ampfuture Co., Ltd. (Shandong, China). Fluorescent quantitative PCR kit for *E. coli* O157:H7 (Cat. HZ-62820) was purchased from Shanghai Huzhen Biotechnology Co. Ltd (Shanghai, China). Fluorescent quantitative PCR kit for SAS-CoV-2 (Cat. Z-RR-0479–02–25) was purchased from Shanghai Liferiver Biotechnology Co., Ltd (Shanghai,

China). Bovine serum albumin (BSA), (3-aminopropyl) triethoxysilane (APTES), and glutaraldehyde of analytical grade were purchased from Sigma-Aldrich (St. Louis, MO, USA). Vortex mixer (VORTEX-6, Kylin-Belll) and thermostat water bath (HCJ-4 A, Jiming) were used. The fluorescence signals of orthogonal CRISPR-Cas12a/Cas13a system were measured using a self-developed all-fiber evanescent wave dual-color fluorescence platform featuring dual-color excitation and detection capabilities (Fig. 1A). Quartz optical fiber ($L = 5.5$ cm, $\Phi = 600$ μm, NA = 0.22) was purchased from Beijing Scitlion Technology Corp., Ltd. The functionalized fiber nano-biosensor was prepared through covalent immobilization of amino-modified cDNA onto the fiber surface via amide bond formation (Fig. 1B). Detailed information is provided in the Supporting Information.

Establishment and characterization of the CD-FOB for parallel detection of E. coli O157:H7 and SARS-CoV-2

The feasibility of individual CRISPR/Cas12a and CRISPR/Cas13a system was verified by detecting different CRISPR/Cas reaction systems via CD-FOB. CRISPR/Cas12a systems with a volume of 20 μL were prepared, which consisted of 50 nM Cas12a, 50 nM Cas12a-crRNA, 1 × Cas12a buffer, *rfbE* gene plasmid, and 500 nM fluorescence reporters (comprising Cy5.5-ssDNA-BHQ3, Cy3-ssRNA-BHQ2, or a mixture of both). Similarly, CRISPR/Cas13a systems, including 50 nM Cas13a, 50 nM Cas13a-crRNA, 1 × Cas13a buffer, SARS-CoV-2 N gene, and 500 nM fluorescence reporters, were also prepared. These mixtures were incubated at 37 ℃ for 60 min and subsequently introduced into the sample cell. Dynamic Cy5.5 and Cy3 fluorescence signals were detected using the dual-color fluorescence analysis platform. The responses of CRISPR/Cas12a system and CRISPR/Cas13a system were displayed by the fluorescence signal in the 635-nm channel for Cy5.5 fluorophores and the 520-nm channel for Cy3 fluorophores, respectively.

The orthogonal Cas12a/Cas13a system was obtained by mixing individual Cas12a and Cas13a systems. Specifically, Cas12a and Cas12a-crRNA, as well as Cas13a and Cas13a-crRNA, were premixed at 37 °C for 30 min to form the Cas12a/crRNA complex and the Cas13a/crRNA complex. Two fluorescence reporters, Cy5.5-ssDNA-BHQ3 and Cy3-ssRNA-BHQ2, were added. Different targets, including *rfbE* gene, N gene, and a mixture of both, were added to the respective reaction mixtures. After incubation for 60 min at 37 °C, the mixtures were analyzed using the dual-color fluorescence analysis platform.

Optimization of CD-FOB detection parameters

Five Cas12a/Cas13a systems with Cas protein concentrations ranging from 10 to 50 nM were incubated at 37 ℃ for 60 min and analyzed by the dual-color fluorescence platform. Several Cas12a/Cas13a systems were prepared with Cas-crRNA ratios of 2:1, 1:1, 1:1.25, 1:1.5, and 1:2, followed by detection after incubated 60 min at 37 ℃. For the formation time of Cas-crRNA, Cas12a-crRNA and Cas13a-crRNA were pre-reacted at 37 ℃ for 5 to 45 min (5-min intervals). Seven buffer formulations (detailed in Table S2) were evaluated using identical reaction protocols, with fluorescence measurements conducted following 60-min incubation. Cas12a/Cas13a systems containing ssDNA/ssRNA reporters at 100–600 nM concentrations (100 nM increments) were tested to determine optimal reporter levels under standard detection conditions. Each concentration was measured in triplicate, with the mean value reported as the detection signal and error bars representing standard deviation (SD).

CD-FOB for parallel detection of E. coli O157:H7 and SARS-CoV-2

Under optimal detection conditions, samples containing varying concentrations of *rfbE* gene and N gene were detected by the CD-FOB method with 40 nM Cas12a/crRNA, 40 nM Cas13a/crRNA, 1 × NBE2.1 buffer, 400 nM ssDNA-reporter, 400 nM ssRNA-reporter, and 8U RNase inhibitor. For intact bacterium and virus, mixed pathogen samples with final concentrations of 500–5×10^6 CFU/mL *E. coli* O157:H7 and 6.45–6.45×10^4 copies/μL FNV-SARS-CoV-2 were analyzed following extraction using a rapid release agent. The mixtures were incubated at 37 ℃ for 60 min and measured by the CD-FOB. The fluorescence signals of a series of samples were fitted with concentrations using four parameter logistic equations.

Simultaneous nucleic acid extraction of E. coli O157:H7 and SARS-CoV-2

The pathogen mixture was prepared by combining equal volumes of phosphate-buffered saline (PBS, pH = 7.4)-diluted *E. coli* O157:H7 (1×10^3–1×10^7 CFU/mL) and FNV-SARS-CoV-2 (12.9–1.29×10^5 copies/μL) suspensions. The concentrations of *E. coli* O157: H7 and FNV-SARS-CoV-2 were pre-quantified using plate counting and qPCR. The mixture was vortexed to achieve thorough mixing before detection. Nucleic acids from *E. coli* O157:H7 and SARS-CoV-2 were co-extracted using a Chelex-100-based rapid release agent in alkaline buffer. Fifty microlitres of the pathogen mixture was mixed with extraction reagent and heated at 95 °C for 5 min to rupture cell membranes and

denature proteins. After centrifugated at 10,000 rpm for 2 min to remove Chelex-100-bound inhibitors (metal ions and nucleases) and equilibrated to room temperature, the supernatant was directly detected by the CD-FOB method with an incubation time of 30 min.

Selectivity of the orthogonal Cas12a/Cas13a detection method

Genomic DNA extracted from several bacteria at concentration of 1×10^8 CFU/mL were used as interference DNA samples, including *Staphylococcus aureus*, *Listeria monocytogenes*, and *Salmonella*. The ORF1ab gene of SARS-CoV-2, ORF1ab gene, and N gene of other coronaviruses including SARS-CoV and MERS-CoV with concentration of 20 nM (10^{10} copies/μL level) were used as interference RNA samples. The orthogonal Cas12a/Cas13a detection method was performed on these interfering components, negative and positive control samples. The specificity was evaluated by the fluorescence signal changes in the 635-nm and 520-nm signal channels.

Parallel detection of E. coli O157:H7 and SARS-CoV-2 in real samples

To investigate the practicality of CD-FOB for the parallel detection of *E. coli* O157:H7 and SARS-CoV-2 in real water samples, tap water samples spiked with *E. coli* O157:H7 and SARS-CoV-2 was prepared. Ten spiked samples comprised four negative controls, two single-positive samples (6×10^4 CFU/mL *E. coli* O157:H7 or 6×10^4 copies/μL SARS-CoV-2), and four dual-positive samples with varying concentrations of both pathogens (*E. coli* O157:H7: 600–1200 CFU/mL; SARS-CoV-2: 100–200 copies/μL). All samples were analyzed by CD-FOB and qPCR following rapid release agent extraction.

Results and discussion

Fabrication and verification of the CD-FOB for parallel detection of E. coli O157:H7 and SARS-CoV-2

The CD-FOB integrates a portable evanescent wave dual-color fluorescence detection device with a functionalized tapered fiber-embedded optofluidic nano-biochip (Fig. 1). The dual-color device employs a single-multimode fiber coupler (SMFC) to simultaneously handle dual-wavelength excitation (520-nm and 635-nm lasers, toggled at 1 Hz via a 2×1 fiber optic switch) and fluorescence signal collection. Two evanescent waves generated on the fiber when two excited lights transmit via total internal reflection that excites Cy3/Cy5.5-labeled reporters. Part of the two wavelengths of fluorescence is coupled back to the fiber and collected by SMFC. A dual-wavelength narrow band filter facilitates the transmission of two fluorescence wavelengths while minimizing cross-talk and scattered excitation light interference. A silicon-based photodiode, PD-1000 detector, is designed and manufactured by our group as a mini-photodetector for parallel detection of the two wavelengths of fluorescence based on the time-resolved effect. The instrument features custom-developed control and data processing software (ANA pro) comprising self-checking, detection/analysis, and communication modules, enabling dual-laser alternating input, real-time dual-fluorescence detection, and fully automated intelligent operation. The device integrates optical detection, biosensing, and data analysis into a compact space (35 cm × 25 cm × 18 cm), achieving > 70% volume reduction versus RT-qPCR while maintaining laboratory-grade accuracy, enabling precise field deployment. The fiber-embedded optofluidic bio-nano-chip is constructed by embedding a functionalized fiber nano-biosensor into an optofluidic chip. A 3D-printed plug-and-play microfluidic chip (1.0 × 6.0 cm) with a 0.6 mm × 3.5 cm microchannel (20-μL volume) was designed. Using a 5.5-cm quartz fiber ($\Phi = 600$ μm, NA = 0.22) with a 3.0-cm sensing part, a nano-porous structure was created through in situ etching via the hydrofluoric acid (HF) tube-etching. The functionalized tapered fiber nano-biosensor was prepared through covalent immobilization of amino-modified cDNA onto the fiber via amide bonding (details in SI).

To achieve parallel detection of *E. coli* O157:H7 and SARS-CoV-2, an orthogonal CRISPR/Cas system was developed based on the different cleavage preferences of Cas12a and Cas13a [31, 44]. For CRISPR/Cas12a system, a significant signal increase was observed in the 635-nm channel only in the presence of both *rfbE* gene and ssDNA-reporter (Fig. 2A). This demonstrated that *rfbE* gene activated the cleavage activity of Cas12a that selectively cleaved Cy5.5-ssDNA-BHQ3 reporters instead of ssRNA-reporter. The cleaved ssDNA-reporter was excited by 635-nm laser rather than 520-nm laser. Similarly, the cleavage preference of Cas13a for ssRNA-reporter was verified by an individual Cas13a system (Fig. 2B). The activated Cas13a by N gene selectively cleaved Cy3-ssRNA-BHQ2 that excited by 520-nm laser, resulting in significant fluorescence signal in the 520-nm channel. When both targets were present, simultaneous dual-channel detection was achieved through time-resolved measurements, with signal responses matching individual system performance (Fig. 2C and 2D). These indicated that the Cas12a and Cas13a system exhibited a different *trans*-cleavage preference, and ssDNA-reporter and ssRNA-reporter were simultaneously detected by CD-FOB based on time-resolved effect without cross-interference. Therefore, the CD-FOB can be applied for parallel detection

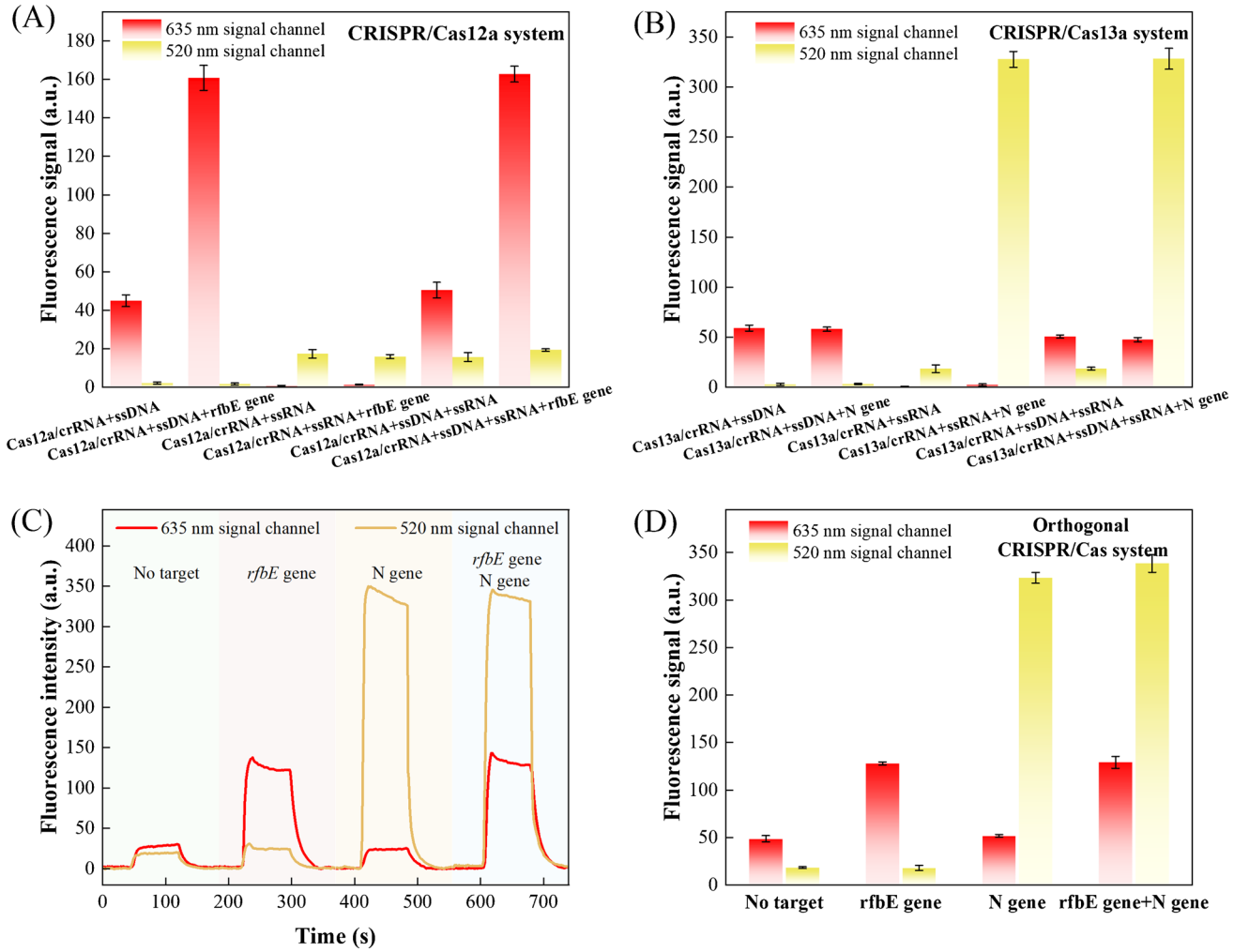

Fig. 2 Feasibility verification of the CD-FOB for parallel detection of *E. coli* O157:H7 and SARS-CoV-2. **A** Verification of the *trans*-cleavage preference of CRISPR/Cas12a system with 50 nM Cas12a, 62.5 nM Cas12a-crRNA, 8.35 $\times 10^7$ copies/μL *rfbE* gene, 500 nM ssDNA-reporter in 1× Cas12a buffer at 37 °C for 1 h; **B** Verification of the *trans*-cleavage preference of CRISPR/Cas13a system with 50 nM Cas13a, 62.5 nM Cas13a-crRNA, 1.2 $\times 10^{10}$ copies/μL N gene, 500 nM ssRNA-reporter in 1× Cas13a buffer at 37 °C for 1 h; **C** Real-time evanescent wave dual-color fluorescence signal traces for orthogonal Cas12a/Cas13a system; **D** Verification of the orthogonal Cas12a/Cas13a system (50 nM Cas12a/crRNA and 50 nM Cas13a/crRNA complex with each ratio of 1:1.25, 8.35 $\times 10^7$ copies/μL *rfbE* gene, 1.2 $\times 10.^{10}$ copies/μL N gene, 500 nM ssRNA-reporter, 500 nM ssDNA-reporter in 1× Cas12a/Cas13a buffer at 37 °C for 1 h). Data represent mean ± SD ($n = 3$)

of *E. coli* O157:H7 and SARS-CoV-2 via the orthogonal CRISPR/Cas system.

The specificity of orthogonal CRISPR-Cas12a/Cas13a system was evaluated by analyzing various pathogen samples, including *Staphylococcus aureus*, *Salmonella*, *Listeria monocytogenes*, SARS-CoV, and Middle East respiratory syndrome virus (MERS-CoV). Results in Fig. S1 showed that the fluorescence responses were measured only in the presence of specific targets (*E. coli* O157:H7 and SARS-CoV-2 N gene), which confirmed the excellent specificity of the orthogonal CRISPR-Cas12a/Cas13a system which stemmed from the inherent high specificity of CRISPR/Cas system and the ingenious signal resolution of the CD-FOB.

Optimization of the orthogonal CRISPR-Cas12a/Cas13a system

To improve the performance of the orthogonal CRISPR-Cas12a/Cas13a system, several key detection parameters were optimized. Figure 3A shows that the cleavage activity of CRISPR/Cas12a increases with increasing Cas12a concentration when it is less than 40 nM, and then reaches a plateau. Increasing the Cas12a concentration did not influence the cleavage activity of CRISPR/Cas13a. Similarly, the cleavage activity of CRISPR/Cas13a increased with increasing Cas13a concentration. However, the cleavage activity of CRISPR/Cas12a was inhibited as Cas13a concentration

exceeded 40 nM (Fig. 3B). Therefore, a moderate reduction in the Cas13a enzyme concentration facilitates the cleavage efficiency of Cas12a assay [45]. The optimal concentration of Cas12a and Cas13a was selected as 40 nM. Figure 3C shows that the fluorescence signal rapidly increased as the ratio of Cas12a or Cas13a to crRNA increased from 2:1 to 1:1.25 and then decreased, making optimized Cas protein/crRNA ratio of 1:1.25. The fluorescence intensity continued to increase over the incubation time of the Cas protein/crRNA mixture, indicating the ongoing response of Cas12a/Cas13a *trans*-cleavage activity (Fig. 3D). Considering the detection period and fluorescence intensity, the incubation time was set to 30 min.

The reaction buffer is critical to obtain good measurement performance for the parallel detection [45, 46]. Figure 3E shows that the cleavage activity of Cas13a significantly decreased in Cas12a buffer, and Cas13a buffer also had a certain inhibitory effect on Cas12a. In a mixture buffer in equal volumes, the cleavage activities of Cas13a and Cas12a are similar to those in the respective buffers. Four other buffers, NEBuffer 1.1, NEBuffer 2.1, NEBuffer 3.1, and CutSmart buffer (details in the SI), were investigated. NEBuffer 2.1 promoted the cleavage activity of Cas12a while maintaining the cleavage activity of Cas13a, and was chosen as the optimal buffer. To determine the optimal concentration of ssDNA/ssRNA reporters, a sensitivity index (ε) was introduced as $\varepsilon = \frac{I_s - I_0}{I_s}$, where I_0 and I_s are the net fluorescence signal of the blank sample and the samples with target. Figure 3F shows that the ε value of Cas12a system initially increased when the ssDNA-reporter was less than 400 nM and then decreased, and the ε value of Cas13a system increased when ssRNA-reporter was less than 500 nM. Considering the sensitivity index, fluorescence intensity, and reagent savings, the optimal ssDNA/ssRNA reporter concentration was determined to be 400 nM. Moreover, the effect of incubation time was also explored and the optimal incubation time was set at 60 min (Fig. S2).

Parallel detection of E. coli O157:H7 and SARS-CoV-2 using CD-FOB with multiple signal enhancement strategy

The performance of the orthogonal Cas12a/Cas13a assay for parallel detection of *rfbE* gene and N gene in homogenous solution was investigated under the optimal conditions. Figure S3A and C display the typical fluorescence curves for various *rfbE* gene and N gene concentrations in the 635-nm channel and 520-nm channel, respectively. The fluorescence signals of the two channels increased with increasing target concentrations, and the detection limit was 279 copies/μL for *rfbE* gene and 3.89×10^3 copies/μL for N gene (Fig. S3B and D). These demonstrated the feasibility of parallel detection of bacterium and virus using CD-FOB, while the LODs of both targets were far from meeting the actual detection needs. Common CRISPR/Cas biosensing systems employed nucleic acid pre-amplification to improve sensitivity, which increases the design complexity, detection period, and cross-contamination risk [47, 48].

A multiple signal enhancement strategy was constructed for ultrasensitive amplification-free detection of *E. coli* O157:H7 and SARS-CoV-2. As shown in Fig. 1B, the first signal enhancement originates from the collateral cleavage amplification effect (exceeding 10,000-fold) of CRISPR/Cas system (Enhancement I). The second signal enhancement is from evanescent wave fluorescence enhancement based on a tapered nano-porous fiber biosensor (Enhancement II). The tapered structure of a fiber amplifies evanescent wave intensity and enhances fluorescence collection efficiency [49]. Additionally, the creation of a nano-porous layer significantly boosts the interaction between the evanescent wave and fluorescent molecules [50]. The existence of nano-porous structures on the surface of optical fiber was characterized by atomic force microscopy (Fig. S4). The third tier of signal enhancement is achieved through DNA-mediated fluorescence enhancement. The fiber nano-biosensor was covalently modified with the cDNA sequence to selectively capture ssDNA-reporter or ssRNA-reporter (Enhancement III in Fig. 1D). The successful modification of the A5 sequence was verified via atomic force microscope (Fig. S4). This A5-capture probe-mediated approach significantly amplifies the fluorescence intensity by 6.1 ~ 9.2 at the same target concentration (Fig. 4A).

An air-displacement fluorescence enhancement strategy was introduced as the fourth level of signal enhancement (Enhancement IV). Following the capture of ssDNA-reporter and ssRNA-reporter on the fiber nano-biosensor surface, air was injected into the optofluidic biochip to displace the solution, which resulted in the emergence of an air signal peak and a significant increase in the fluorescence intensity (Fig. 4A). This enhancement can be attributed to two primary factors. First, when the solution was replaced with air, the V number, a dimensionless parameter that determines the mode capacity of the fiber, increased by 1.8 times because the lower refractive index of air [51]. The increased V number allows for the transmission of a greater amount of mode excitation light into the tapered fiber nano-biosensor, significantly enhancing the evanescent wave intensity at the interface and improving the excitation efficiency. Second, the increased V number also enhances the coupling efficiency of the excited fluorescence, as most of the excited light consists of high-order mode light. These factors collectively contribute to a higher fluorescence intensity. By integrating the four described fluorescence signal enhancement effects, we

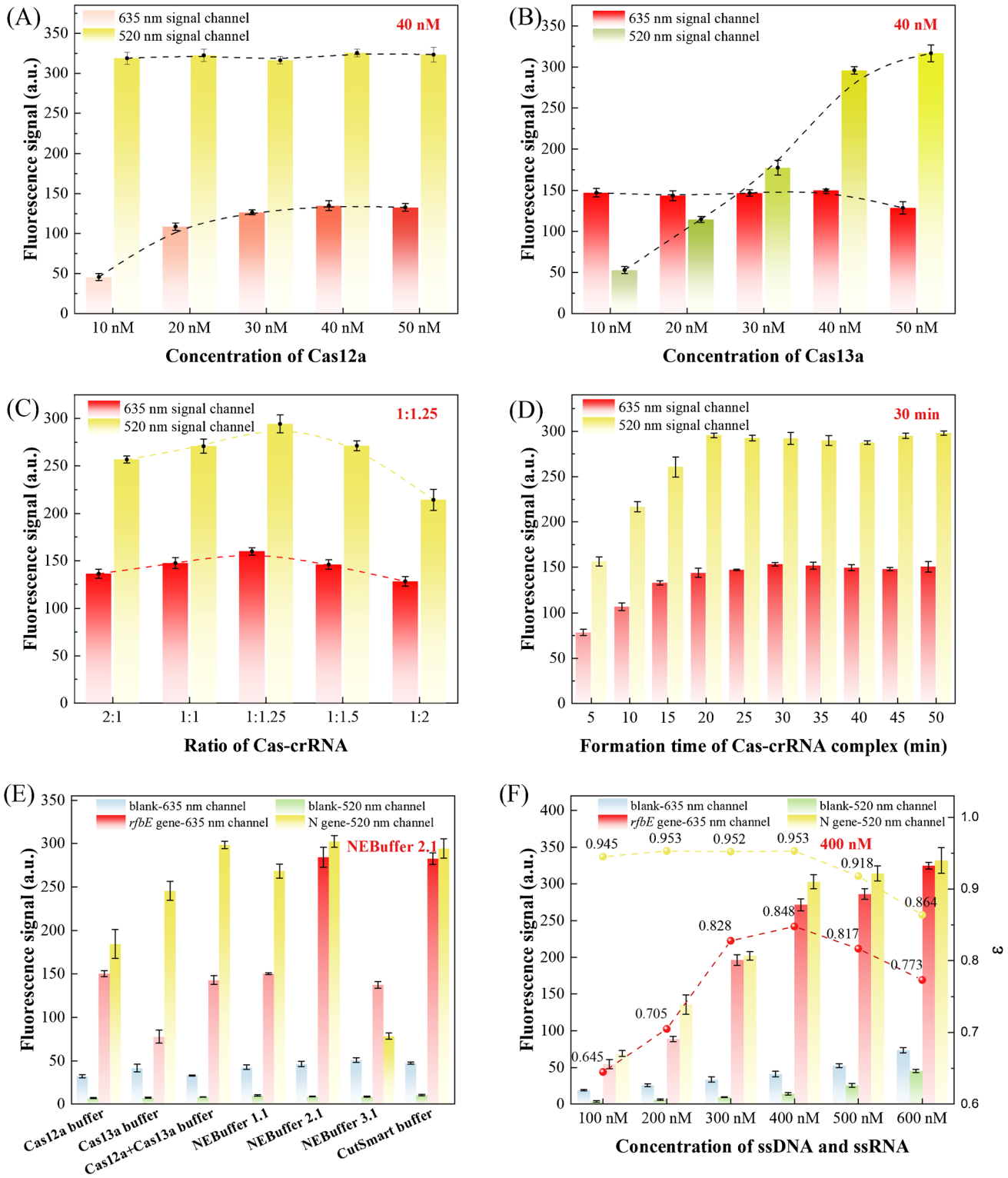

anticipate that CD-FOB will achieve ultrasensitive pathogen detection without the need for nucleic acid amplification.

As shown in Fig. 4A and B, increasing the target concentration increased the amount of cleaved ssDNA-reporter and ssRNA-reporter, thus resulting in the increasing fluorescence signals in the two channels. Figure 4C and D show the concentration–response curves of *rfbE* gene and N gene in solution, respectively. The LODs of *rfbE* gene and N gene were determined to be 44.3 copies/μL ($R^2 = 0.993$) and 33.7 copies/μL ($R^2 = 0.996$), respectively, with the signal in solution

◂**Fig. 3** Optimization of reaction conditions of the orthogonal CRISPR-Cas12a/Cas13a system. **A** Cas12a concentration from 10 to 50 nM with ratio of 1:1.25 Cas12a-crRNA, 50 nM Cas13a/crRNA complex with ratio of 1:1.25, 500 nM ssRNA/ssDNA reporters in 1× Cas12a/Cas13a buffer; **B** Cas13a concentration from 10 to 50 nM with ratio of 1:1.25 Cas13a-crRNA, 50 nM Cas12a/crRNA complex with ratio of 1:1.25, 500 nM ssRNA/ssDNA reporters in 1× Cas12a/Cas13a buffer; **C** Cas-crRNA ratio from 2:1 to 1:2 with 40 nM Cas12a/crRNA complex, 40 nM Cas13a/crRNA complex, 500 nM ssRNA/ssDNA reporters in 1× Cas12a/Cas13a buffer; **D** Formation time of Cas-crRNA complex from 5 to 50 min with 40 nM Cas/crRNA complex, 500 nM ssRNA/ssDNA reporters in 1× Cas12a/Cas13a buffer; **D** Reaction buffer with detailed descriptions in Supplementary Information; **E** Concentration of fluorescent reporters from 100 to 600 nM with 40 nM Cas12/crRNA complex in 1× NEBuffer 2.1. Basic reaction conditions were 8.35 $\times 10^7$ copies/μL *rfbE* gene, 1.2 $\times 10.^{10}$ copies/μL N gene at 37 °C for 1 h. Data represent mean ± SD ($n = 3$)

based on 3σ. The LODs of *rfbE* gene and N gene improved 6.29 and 115 times better compared with those only with the collateral cleavage amplification effect of CRISPR/Cas system. Furthermore, with displacement of air/solution, the LODs of *rfbE* gene and N gene were determined to be 1.15 copies/μL ($R^2 = 0.997$) and 4.19 copies/μL ($R^2 = 0.990$), respectively, with the signal in air based on 3σ (Fig. 4E and F). The LODs of both targets further enhanced 38.5 and 8.04 times than those in solution. These results confirmed the excellent improvement in detection sensitivity using the multiple signal amplification strategies. Moreover, the functionalized tapered fiber-embedded optofluidic nano-biochip demonstrated reusability for up to 70 detection cycles (Fig. S5), significantly improving detection accuracy while reducing costs and waste. Notably, clinical diagnostic devices for intact infectious pathogens mush remain disposable to prevent infection risks. However, for non-infectious targets, such as glucose in clinical diagnostics or environment pollutants, reusable biosensor technology offers substantial advantages, including higher throughout and lower costs [52–54]. In this work, nucleic acids were extracted for testing only after viral and bacterial inactivation, ensuring non-infectious samples. This reusability feature effectively minimizes testing expenses without compromising safety.

Rapid detection of E. coli O157:H7 and SARS-CoV-2 using CD-FOB

To verify the analytical performance of CD-FOB, nucleic acids of *E. coli* O157:H7 and SARS-CoV-2 were extracted using rapid release agent. Owing to the limitations of experimental conditions, a synthetic SARS-CoV-2 pseudovirus (FNV-SARS-CoV-2-abEN, referred as SARS-CoV-2) was used as a substitute. The extracted nucleic acid was simultaneously detected by the CD-FOB and qPCR. After the validation of purified nucleic acids (Fig. 4), the method successfully detected target sequences in complex bacterial and viral lysates from intact bacteria and viruses (Fig. 5), exhibiting remarkable resistance to matrix interference while maintaining detection sensitivity. As shown in Fig. 5, the detection limits of *E. coli* O157:H7 and SARS-CoV-2 were 643 CFU/mL and 3.48 copies/μL for the CD-FOB based on a multiple signal amplification strategy. These results are similar with those of qPCR with LODs of 447 CFU/mL for *E. coli* O157:H7 and 4.5 copies/μL for SARS-CoV-2 based on the standard that Ct value of 35 (Fig. S6). Notably, the qPCR method detected two targets separately because the multiplex PCR system requires complex design of primers and probes to avoid nonspecific amplification. However, the orthogonal CRISPR−Cas12a/Cas13a system achieved parallel detection in one tube and effectively avoided contamination problems due to amplification-free performance. As shown in Table S4, the proposed method demonstrated significant advantages in terms of quantitative capability, operational complexity, device portability, and detection costs compared with other multiplexed CRISPR/Cas systems based on multiple Cas effectors [32, 45, 55]. Given the growing demand for rapid, multiplex pathogen diagnostics, especially in outbreaks and low-resource settings, the CD-FOB's simplicity, robustness, cost-effectiveness, and scalability position it as a promising tool for current and emerging infectious threats.

Evaluation of the lyophilized orthogonal Cas12a/Cas13a system

To achieve "sample to result" on-site analysis of pathogens, a lyophilized orthogonal CRISPR-Cas12a/Cas13a system was prepared via the freeze-drying technique. The components of freeze-drying protective reagents (detailed in Table S3) were optimized. Figure 6A and Fig. S7 show that formula H, consisting of 20 μL CRISPR reaction system, 15 μL (10% trehalose, 10% pullulan, 10% glycine), and 5 μL 30% mannitol (Fig. 6), can maintain the best performance of the CRISPR/Cas12a and CRISPR/Cas13a system. Therefore, formula H was used to produce the lyophilized orthogonal Cas12a/Cas13a reagents. The analytical consistency and preservation performance were evaluated. The fluorescence signals of the 15 groups of lyophilized products from three batches exhibited variation coefficients within 2.3% (Fig. 6D). As the storage time increased at room temperature, the signal of the blank system remained unchanged, which confirmed the stability of the fluorescent probe (Fig. 6E). During 0–3 weeks, the activity of Cas effectors remained stable; however, the Cas12a activity decreased significantly from the 4 th week, whereas the Cas13a activity remained stable after a decrease. Results indicated that storage at 37 °C caused more activity loss compared with storage at room temperature (Fig. S8). The stability of storage

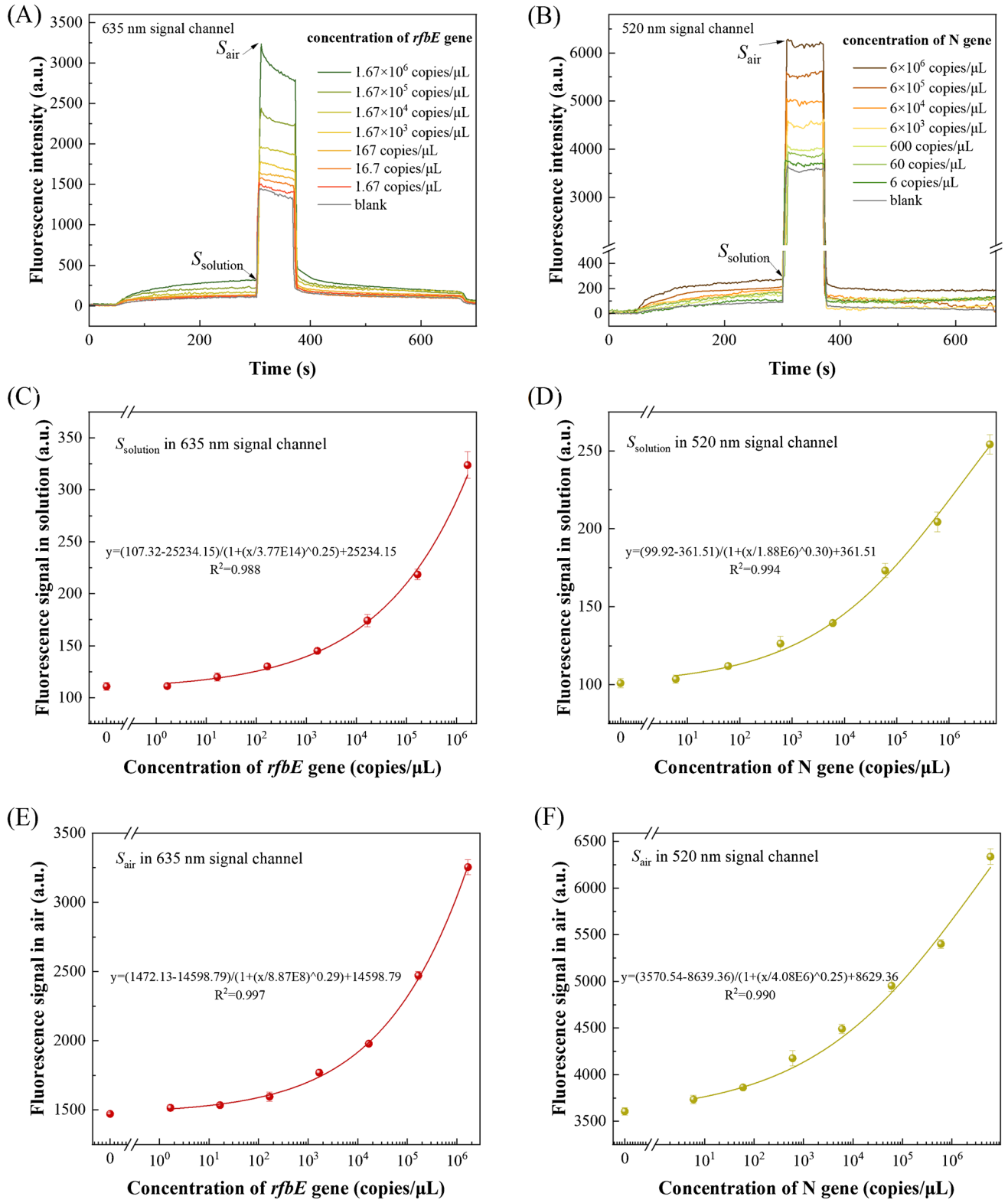

Fig. 4 **A, B** Typical fluorescence curves of the orthogonal Cas12a/Cas13a detection system for simultaneous detection of *rfbE* gene and N gene based on multiple signal enhancement strategy; **C, D** Concentration–response curves for series concentration of *rfbE* gene and N gene with the fluorescence signal in solution; **E, F** Concentration–response curves for series concentration of *rfbE* gene and N gene with the fluorescence signal in air. Reaction condition was 40 nM Cas/crRNA complex with ratio of 1:1.25, 400 nM ssRNA/ssDNA reporters in NEBuffer 2.1 at 37 °C for 30 min. Data represent mean ± SD ($n = 3$)

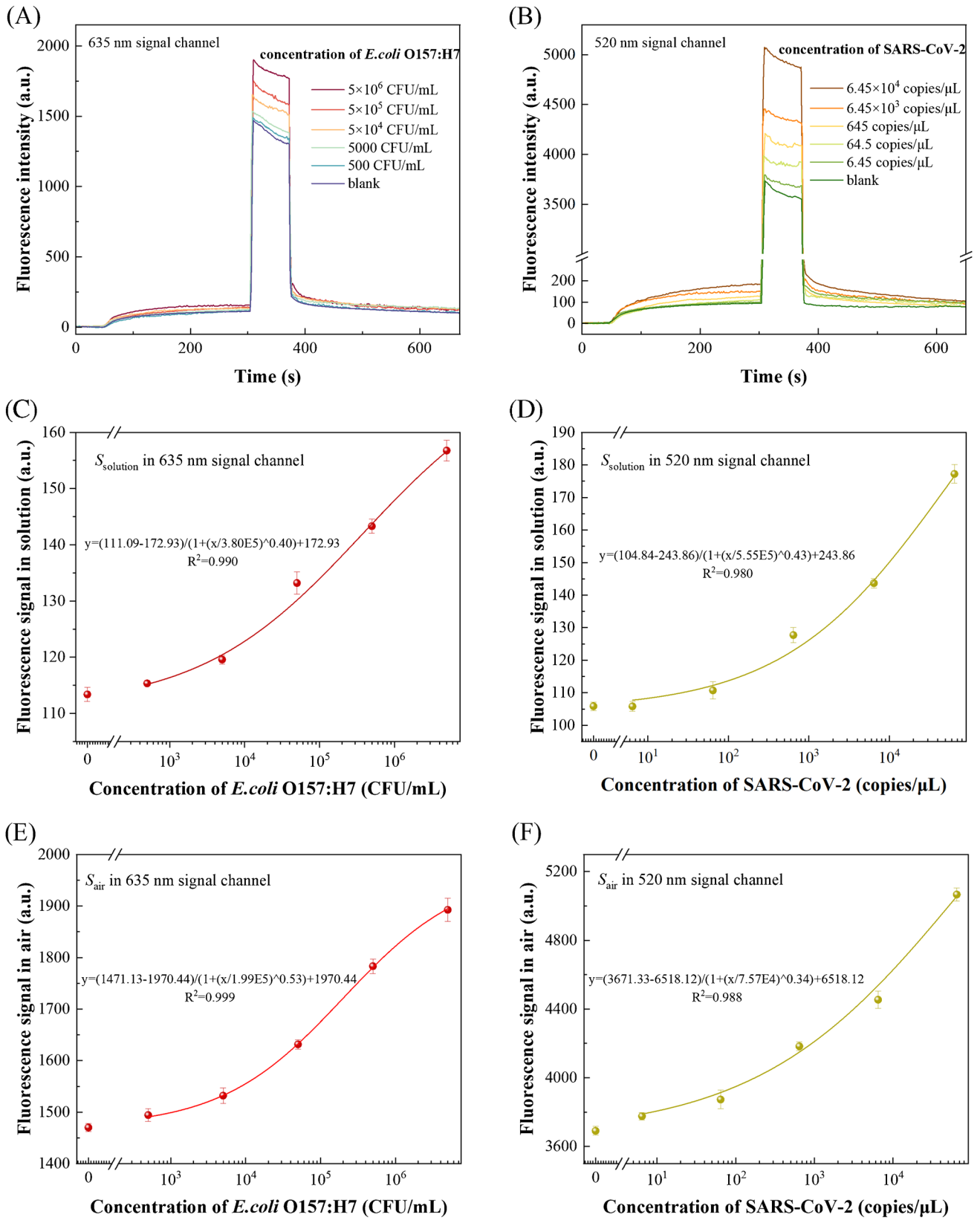

Fig. 5 Typical fluorescence curves of the orthogonal Cas12a/Cas13a detection system for simultaneous detection of (**A**) *E. coli* O157:H7 in 635-nm channel and (**B**) SARS-CoV-2 in 520-nm channel; **C, D** Concentration–response curves for a series concentration of *E. coli* O157:H7 and SARS-CoV-2 with the fluorescence signal in solution; **E, F** Concentration–response curves for a series concentration of *E. coli* O157:H7 and SARS-CoV-2 with the fluorescence signal in air. Data represent mean ± SD ($n = 3$)

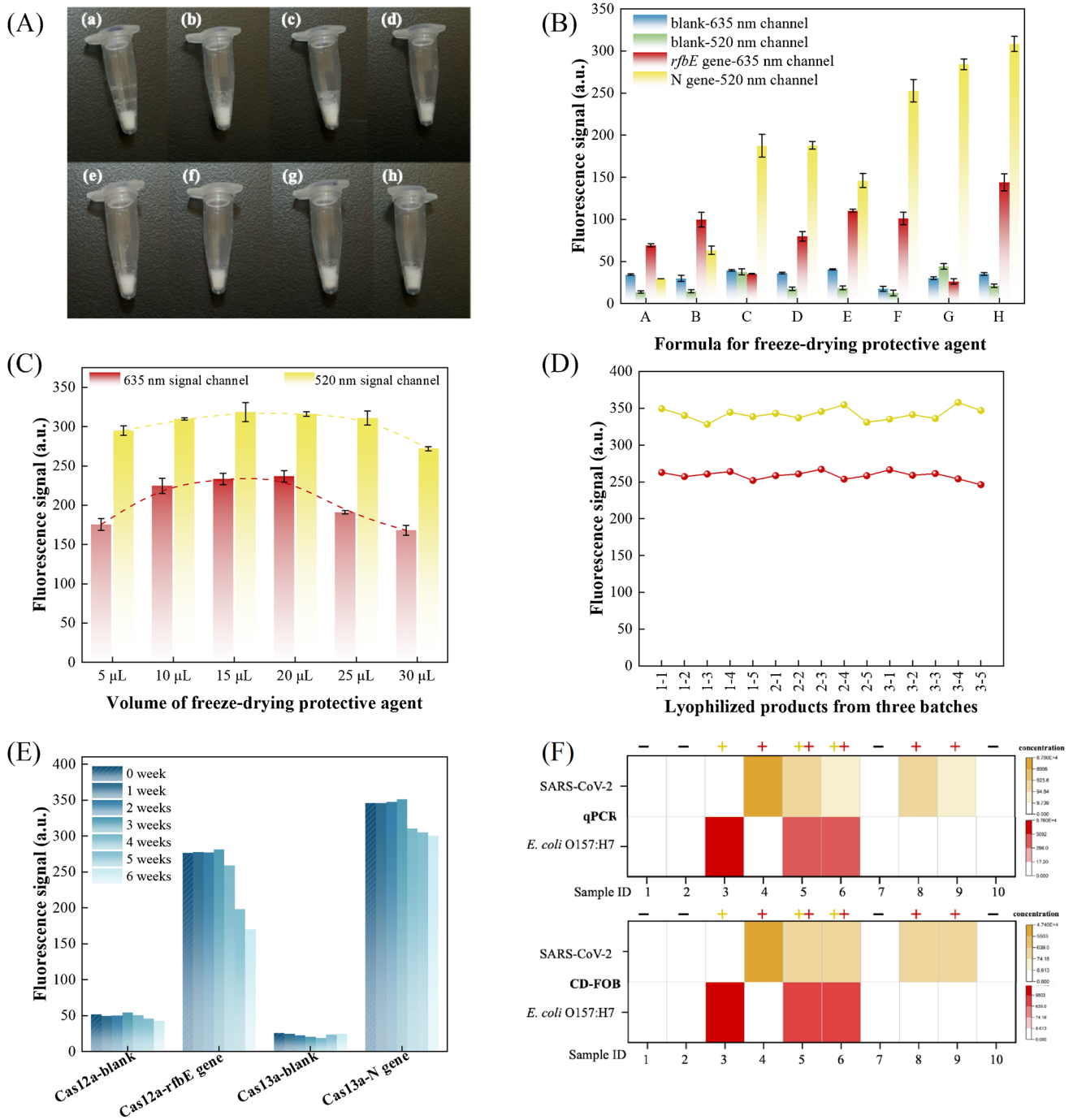

Fig. 6 Evaluation of the lyophilized orthogonal Cas12a/Cas13a system. **A** Pictures of freeze-dried products using orthogonal Cas12a/Cas13a detection systems with different freeze-drying formulas; **B** Detection performance of freeze-dried products with different freeze-drying formulas; **C** Optimization of the freeze-drying protective agent volume; **D** Characterization of detection performance of freeze-dried products from different batches; **E** Detection performance of freeze-dried reagents under different storage times; **F** Detection results of *E. coli* O157:H7 and SARS-CoV-2 in 10 water environment samples using CD-FOB and qPCR methods. Data represent mean ± SD ($n = 3$)

at room temperature allows it to completely overcome the limitations of cold chain transportation, facilitating long-distance transportation and long-term storage at room temperature, and is more suitable for timely on-site testing. Further long-term storage stability of freeze-drying reagents (e.g., 6 months and 1 year) could be explored in the future work.

Detection of real samples using CD-FOB and lyophilized reagents

Spiked water with different concentrations of *E. coli* O157:H7 and SARS-CoV-2 was prepared as the actual environmental samples. After extraction with the rapid release agent, the supernatant was directly detected using the orthogonal CRISPR−Cas12a/Cas13a method and the qPCR method. The results are presented in Table S5. As shown in Fig. 6F, both the proposed method and qPCR method effectively detected positive and negative samples. The recovery rates of the qPCR method were 130.8%–226.0% for *E. coli* O157:H7 and 70.4%–145.9% for SARS-CoV-2. For the proposed method, the recovery rates for *E. coli* O157:H7 and SARS-CoV-2 were between 70.5%–200.5% and 81.4%–162.7%, which was consistent with the results of the qPCR method. Alongside high accuracy, the CD-FOB method also exhibited showing excellent precision for rapid on-site simultaneous detection of *E. coli* O157:H7 and SARS-CoV-2 with RSD value below 10.4%. These findings indicate that the proposed method can be employed for rapid on-site simultaneous detection of *E. coli* O157:H7 and SARS-CoV-2. The proposed method shows significant cost advantages compared to conventional RT-qPCR method (Table S6). With cost-effectiveness, quantitative capability, easy-operation, and portability, the CD-FOB method demonstrates strong potential for rapid parallel on-site detection of bacterial and viral pathogens.

Despite the above strengths and opportunities, several technical and practical challenges deserve consideration. The matrix effects from complex clinical specimens (e.g., blood) may contain nucleases or other interferents that could potentially compromise CRISPR/Cas activity, which has high requirements for the nucleic acid extraction effect. Besides, the reliability for monitoring waterborne pathogens in complex environmental samples (e.g., concentrated wastewater) remains to be thoroughly validated. While the system excels in dual-pathogen detection, scaling to broader panels may face challenges in CRISPR orthogonality and signal cross-talk. Competing technologies (e.g., isothermal amplification or portable device) could outpace its adoption if they offer faster or cheaper solutions. Further optimization of reagent stability, cost reduction, and validation in diverse clinical/environmental samples will be critical to ensure widespread utility and competitiveness.

Conclusions

In conclusion, a CD-FOB system was developed for parallel on-site detection of *E. coli* O157:H7 and SARS-CoV-2 combining the advantages of evanescent wave dual-color fluorescence detection device, orthogonal CRISPR/Cas system, and tapered fiber-embedded optofluidic nano-biochip. The employment of a multiple signal enhancement strategy achieved high sensitivity, with LOD values of 643 CFU/mL and 3.48 copies/μL for *E. coli* O157:H7 and SARS-CoV-2, which eliminates the dependence on time-consuming pre-amplification. Taking advantage of the rapid release reagent, parallel detection of two pathogens was accomplished within 50 min, which almost 60% reduction compared to conventional CRISPR-based workflows. Furthermore, lyophilized reagents with high stability and consistency were prepared to facilitate on-site detection. Successful analysis of actual water samples demonstrated the good applicability and prospects of the proposed method. Therefore, this method exhibits obvious advantages, including multiplexed detection ability, portable equipment, and simple operation, which offers potentially powerful solutions for the development of accurate, low-cost, and user-friendly multiplexed CRISPR diagnostics. Despite its advantages, the CD-FOB system faces challenges and limitations, including potential interference from complex clinical or environmental samples, limitations in scaling to broader pathogen panels, and competition from alternative technologies. Further optimization of nucleic acid extraction, reagent stability, and cost-effectiveness, along with extensive validation in diverse samples, will be essential to enhance its practical utility and competitiveness.

Supplementary Information The online version contains supplementary material available at https://doi.org/10.1007/s00604-025-07289-5.

Author contribution Dan Song: Conceptualization, Methodology, Validation, Writing-original draft, Funding acquisition. Wenjuan Xu and Yuxin Zhuo: Methodology, Investigation. Anna Zhu: Project administration, Writing-review & editing. Feng Long: Supervision, Funding acquisition, Methodology, Writing-review & editing.

Funding This work was supported by the Natural Science Foundation of Beijing (8242031) and the National Key R&D Program of China (2022YFF0609102).

Data availability No datasets were generated or analysed during the current study.

Declarations

Ethics declaration Not applicable.

Conflict of interest The authors declare no competing interests.

References

1. Calderon M, Gysin G, Gujjar A et al (2023) Bacterial co-infection and antibiotic stewardship in patients with COVID-19: a systematic review and meta-analysis. BMC Infect Dis 23:14. https://doi.org/10.1186/s12879-022-07942-x
2. Dong Y, Jiang Z, Hu Y et al (2024) Pathogen contamination of groundwater systems and health risks. Crit Rev Environ Sci

Technol 54:267–289. https://doi.org/10.1080/10643389.2023.2236486
3. Su Y, Gao R, Huang F et al (2024) Occurrence, transmission and risks assessment of pathogens in aquatic environments accessible to humans. J Environ Manage 354:120331. https://doi.org/10.1016/j.jenvman.2024.120331
4. Zhu D, Zhang Y, Zhu Y-G (2023) Human pathogens in the soil ecosystem: occurrence, dispersal, and study method. Curr Opin Environ Sci Health 33:100471. https://doi.org/10.1016/j.coesh.2023.100471
5. Lian S, Liu J, Wu Y et al (2022) Bacterial and viral co-infection in the intestine: competition scenario and their effect on host immunity. IJMS 23:2311. https://doi.org/10.3390/ijms23042311
6. Pokhrel V, Kuntal BK, Mande SS (2024) Role and significance of virus-bacteria interactions in disease progression. J Appl Microbiol 135:lxae130. https://doi.org/10.1093/jambio/lxae130
7. Sun K, Metzger DW (2008) Inhibition of pulmonary antibacterial defense by interferon-γ during recovery from influenza infection. Nat Med 14:558–564. https://doi.org/10.1038/nm1765
8. Li N, Ren A, Wang X et al (2015) Influenza viral neuraminidase primes bacterial coinfection through TGF-β–mediated expression of host cell receptors. Proc Natl Acad Sci USA 112:238–243. https://doi.org/10.1073/pnas.1414422112
9. Bellinghausen C, Gulraiz F, Heinzmann ACA et al (2016) Exposure to common respiratory bacteria alters the airway epithelial response to subsequent viral infection. Respir Res 17:68. https://doi.org/10.1186/s12931-016-0382-z
10. Barman TK, Singh AK, Bonin JL et al (2022) Lethal synergy between SARS-CoV-2 and Streptococcus pneumoniae in hACE2 mice and protective efficacy of vaccination. JCI Insight 7:e159422. https://doi.org/10.1172/jci.insight.159422
11. Moon S, Han S, Jang I-H et al (2024) Airway epithelial CD47 plays a critical role in inducing influenza virus-mediated bacterial super-infection. Nat Commun 15:3666. https://doi.org/10.1038/s41467-024-47963-5
12. Avadhanula V, Rodriguez CA, DeVincenzo JP et al (2006) Respiratory viruses augment the adhesion of bacterial pathogens to respiratory epithelium in a viral species- and cell type-dependent manner. J Virol 80:1629–1636. https://doi.org/10.1128/JVI.80.4.1629-1636.2006
13. Rowe HM, Rosch JW (2019) Close encounters of the viral kind: cross-kingdom synergies at the host–pathogen interface. BioEssays 41:1900128. https://doi.org/10.1002/bies.201900128
14. Rowe HM, Meliopoulos VA, Iverson A et al (2019) Direct interactions with influenza promote bacterial adherence during respiratory infections. Nat Microbiol 4:1328–1336. https://doi.org/10.1038/s41564-019-0447-0
15. Morens DM, Taubenberger JK, Fauci AS (2008) Predominant role of bacterial pneumonia as a cause of death in pandemic influenza: implications for pandemic influenza preparedness. J Infect Dis 198:962–970. https://doi.org/10.1086/591708
16. Alqahtani A, Alamer E, Mir M et al (2022) Bacterial coinfections increase mortality of severely ill COVID-19 patients in Saudi Arabia. IJERPH 19:2424. https://doi.org/10.3390/ijerph19042424
17. Akbari Nakhjavani S, Mirzajani H, Carrara S, Onbaşlı MC (2024) Advances in biosensor technologies for infectious diseases detection. TrAC Trends Anal Chem 180:117979. https://doi.org/10.1016/j.trac.2024.117979
18. Liu Q, Jin X, Cheng J et al (2023) Advances in the application of molecular diagnostic techniques for the detection of infectious disease pathogens (Review). Mol Med Rep 27:104. https://doi.org/10.3892/mmr.2023.12991
19. Zhao Y, Zhang W, Zhang X (2024) Application of metagenomic next-generation sequencing in the diagnosis of infectious diseases. Front Cell Infect Microbiol 14:1458316. https://doi.org/10.3389/fcimb.2024.1458316
20. Artika IM, Dewi YP, Nainggolan IM et al (2022) Real-time polymerase chain reaction: current techniques, applications, and role in COVID-19 diagnosis. Genes 13:2387. https://doi.org/10.3390/genes13122387
21. Kreitmann L, Miglietta L, Xu K et al (2023) Next-generation molecular diagnostics: leveraging digital technologies to enhance multiplexing in real-time PCR. TrAC, Trends Anal Chem 160:116963. https://doi.org/10.1016/j.trac.2023.116963
22. Sharma S, Shrivastava S, Kausley SB, Rai B (2023) Integrated point-of-care RT-PCR methods during and after COVID-19 pandemic. VirusDis 34:356–364. https://doi.org/10.1007/s13337-023-00834-x
23. Akarapipad P, Bertelson E, Pessell A et al (2022) Emerging multiplex nucleic acid diagnostic tests for combating COVID-19. Biosensors 12:978. https://doi.org/10.3390/bios12110978
24. Yang J, Li D, Wang J et al (2022) Design, optimization, and application of multiplex rRT-PCR in the detection of respiratory viruses. Crit Rev Clin Lab Sci 59:555–572. https://doi.org/10.1080/10408363.2022.2072467
25. Miao G, Jiang X, Yang D et al (2022) A hand-held, real-time, AI-assisted capillary convection PCR system for point-of-care diagnosis of African swine fever virus. Sens Actuators B Chem 358:131476. https://doi.org/10.1016/j.snb.2022.131476
26. Staniszewski F, Schilder A, Osinkina L et al (2024) Rapid detection of SARS-CoV-2 with a mobile device based on pulse controlled amplification. Biosens Bioelectron 263:116626. https://doi.org/10.1016/j.bios.2024.116626
27. Dmytrenko O, Neumann GC, Hallmark T et al (2023) Cas12a2 elicits abortive infection through RNA-triggered destruction of dsDNA. Nature 613:588–594. https://doi.org/10.1038/s41586-022-05559-3
28. Gleerup JL, Mogensen TH (2022) CRISPR-Cas in diagnostics and therapy of infectious diseases. J Infect Dis 226:1867–1876. https://doi.org/10.1093/infdis/jiac145
29. Masi A, Antonacci A, Moccia M et al (2023) CRISPR-Cas assisted diagnostics: a broad application biosensing approach. TrAC Trends Anal Chem 162:117028. https://doi.org/10.1016/j.trac.2023.117028
30. De Puig H, Lee RA, Najjar D et al (2021) Minimally instrumented SHERLOCK (miSHERLOCK) for CRISPR-based point-of-care diagnosis of SARS-CoV-2 and emerging variants. Sci Adv 7:eabh2944. https://doi.org/10.1126/sciadv.abh2944
31. Gootenberg JS, Abudayyeh OO, Lee JW et al (2017) Nucleic acid detection with CRISPR-Cas13a/C2c2. Science 356:438–442. https://doi.org/10.1126/science.aam9321
32. Guk K, Yi S, Kim H et al (2023) Hybrid CRISPR/Cas protein for one-pot detection of DNA and RNA. Biosens Bioelectron 219:114819. https://doi.org/10.1016/j.bios.2022.114819
33. Jiang T, Liu R, Shen J (2023) CRISPR dual enzyme cleavage triggers DNA and RNA substrate cleavage for SARS-CoV-2 dual gene detection. J Med Virol 95:e29090. https://doi.org/10.1002/jmv.29090
34. Gootenberg JS, Abudayyeh OO, Kellner MJ et al (2018) Multiplexed and portable nucleic acid detection platform with Cas13, Cas12a, and Csm6. Science 360:439–444. https://doi.org/10.1126/science.aaq0179
35. Liu F, An T, Zhou C et al (2024) Amplification-free orthogonal CRISPR/Cas system for rapid discrimination of bacterial vs viral infection in febrile children. Sens Actuators B Chem 418:136319. https://doi.org/10.1016/j.snb.2024.136319
36. Zalke JB, Bhaiyya ML, Jain PA et al (2024) A machine learning assisted non-enzymatic electrochemical biosensor to detect urea based on multi-walled carbon nanotube functionalized with copper oxide micro-flowers. Biosensors 14:504. https://doi.org/10.3390/bios14100504

37. Choi J-H, Lim J, Shin M et al (2021) CRISPR-Cas12a-based nucleic acid amplification-free DNA biosensor via Au nanoparticle-assisted metal-enhanced fluorescence and colorimetric analysis. Nano Lett 21:693–699. https://doi.org/10.1021/acs.nanolett.0c04303
38. Tong G, Nath P, Hiruta Y, Citterio D (2025) Amplification-free CRISPR/Cas based dual-enzymatic colorimetric nucleic acid biosensing device. Lab Chip 25:536–545. https://doi.org/10.1039/D4LC01039F
39. Rahman M, Islam KR, Islam MdR et al (2022) A critical review on the sensing, control, and manipulation of single molecules on optofluidic devices. Micromachines 13:968. https://doi.org/10.3390/mi13060968
40. Stollmann A, Garcia-Guirado J, Hong J-S et al (2024) Molecular fingerprinting of biological nanoparticles with a label-free optofluidic platform. Nat Commun 15:4109. https://doi.org/10.1038/s41467-024-48132-4
41. Xie F, Liang L, Zhao C et al (2025) Parallel optofluidic detection of multiple cardiac biomarkers for point-of-care testing applications. Opt Laser Technol 180:111504. https://doi.org/10.1016/j.optlastec.2024.111504
42. Bhatt A, Dada AC, Prajapati SK, Arora P (2023) Integrating life cycle assessment with quantitative microbial risk assessment for a holistic evaluation of sewage treatment plant. Sci Total Environ 862:160842. https://doi.org/10.1016/j.scitotenv.2022.160842
43. Gwenzi W, Adelodun B, Kumar P et al (2024) Human viral pathogens in the wastewater-source water-drinking water continuum: evidence, health risks, and lessons for future outbreaks in low-income settings. Sci Total Environ 918:170214. https://doi.org/10.1016/j.scitotenv.2024.170214
44. Chen JS, Ma E, Harrington LB et al (2018) CRISPR-Cas12a target binding unleashes indiscriminate single-stranded DNase activity. Science 360:436–439. https://doi.org/10.1126/science.aar6245
45. Tian T, Qiu Z, Jiang Y et al (2022) Exploiting the orthogonal CRISPR-Cas12a/Cas13a trans-cleavage for dual-gene virus detection using a handheld device. Biosens Bioelectron 196:113701. https://doi.org/10.1016/j.bios.2021.113701
46. Lv H, Wang J, Zhang J et al (2021) Definition of CRISPR Cas12a trans-cleavage units to facilitate CRISPR diagnostics. Front Microbiol 12:766464. https://doi.org/10.3389/fmicb.2021.766464
47. Mao X, Xu M, Luo S et al (2023) Advancements in the synergy of isothermal amplification and CRISPR-cas technologies for pathogen detection. Front Bioeng Biotechnol 11:1273988. https://doi.org/10.3389/fbioe.2023.1273988
48. Zeng D, Jiao J, Mo T (2024) Combination of nucleic acid amplification and CRISPR/Cas technology in pathogen detection. Front Microbiol 15:1355234. https://doi.org/10.3389/fmicb.2024.1355234
49. Fang S, Song D, Zhuo Y et al (2021) Simultaneous and sensitive determination of Escherichia coli O157:H7 and Salmonella typhimurium using evanescent wave dual-color fluorescence aptasensor based on micro/nano size effect. Biosens Bioelectron 185:113288. https://doi.org/10.1016/j.bios.2021.113288
50. Lijing Z, Zakoldaev RA, Sergeev MM, Veiko VP (2020) Fluorescent bulk waveguide sensor in porous glass: concept, fabrication, and testing. Nanomaterials 10:2169. https://doi.org/10.3390/nano10112169
51. Han X, Song D, Xu W et al (2024) CRISPR/Cas12a powered air-displacement enhanced evanescent wave fluorescence fiber-embedded microfluidic biochip for nucleic acid amplification-free detection of Escherichia coli O157:H7. J Hazard Mater 469:134037. https://doi.org/10.1016/j.jhazmat.2024.134037
52. Yue W, Kim E-S, Ganbold E et al (2023) A miniature and reusable radiofrequency biosensor combining microfluidic and integrated passive technology for glucose detection. Sens Actuators B Chem 392:134108. https://doi.org/10.1016/j.snb.2023.134108
53 Forinová M, Pilipenco A, Lynn NS et al (2024) A reusable QCM biosensor with stable antifouling nano-coating for on-site reagent-free rapid detection of E. coli O157:H7 in food products. Food Control 165:110695. https://doi.org/10.1016/j.foodcont.2024.110695
54. Liu R, Li Y, Liu Y et al (2025) A highly sensitive and reusable magnetic nano-electrochemical biosensor for the detection of the liver cancer biomarker heat shock protein 70. Chem Eng J 505:159860. https://doi.org/10.1016/j.cej.2025.159860
55. Su G, Zhu M, Li D et al (2022) Multiplexed lateral flow assay integrated with orthogonal CRISPR-Cas system for SARS-CoV-2 detection. Sens Actuators B Chem 371:132537. https://doi.org/10.1016/j.snb.2022.132537